

# Universal Approximation with XL MIMO Systems: OTA Classification via Trainable Analog Combining

Kyriakos Stylianopoulos and George C. Alexandropoulos

Department of Informatics and Telecommunications, National and Kapodistrian University of Athens

Panepistimiopolis Ilissia, 16122 Athens, Greece

emails: {kstylianop, alexandg}@di.uoa.gr

**Abstract**—In this paper, we demonstrate that an eXtremely Large (XL) Multiple-Input Multiple-Output (MIMO) wireless system with appropriate analog combining components exhibits the properties of a universal function approximator, similar to a feedforward neural network. By treating the XL MIMO channel coefficients as the random nodes of a hidden layer, and the receiver’s analog combiner as a trainable output layer, we cast the end-to-end system to the Extreme Learning Machine (ELM) framework, leading to a novel formulation for Over-The-Air (OTA) edge inference without requiring traditional digital processing nor pre-processing at the transmitter. Through theoretical analysis and numerical evaluation, we showcase that XL-MIMO-ELM enables near-instantaneous training and efficient classification, suggesting the paradigm shift of beyond massive MIMO systems as neural networks alongside their profound communications role. Compared to deep learning approaches and conventional ELMs, the proposed framework achieves on par performance with orders of magnitude lower complexity, making it highly attractive for ultra low power wireless devices.

**Index Terms**—Extreme learning machines, XL MIMO, over-the-air computing, analog combining, universal approximation.

## I. INTRODUCTION

Wireless propagation effects are being lately exploited to provide a computational medium towards wave-domain computing [1]. Notably, all-analog Over-The-Air (OTA) implementations of artificial neural networks have been recently proposed in [2], [3], offering a promising direction for energy-efficient Machine Learning (ML). However, up-to-date demonstrations are precisely developed on controlled (clutter-free) radio propagation environments, which limits their relevance to emerging large-scale applications and increases associated costs. In fact, the widespread adoption of OTA ML-based tasks in industrial wireless systems and use cases necessitates hardware compatibility with the existing infrastructure and relevant radio propagation environments.

In the context of wireless communications, OTA-based deep learning has been exploited under the framework of Goal-Oriented (GO) communications for edge inference [4], [5]. In particular, existing GO frameworks split deep neural networks across transceiver devices [6], so that only goal-specific learned features are transmitted by the Transmitter (Tx), enabling the Receiver (Rx) to infer the target information from each data observation. Under this treatment, GO approaches

balance computational and communication constraints, lately leveraging metasurfaces-enabled smart wireless propagation environments [5], [7]. Nevertheless, they require extensive offline training and are tied to specific channel conditions, which degrades their performance under dynamic environments. Thus, efficient GO communications require inference methods that adapt to rapidly changing conditions and are re-trained with minimal computational burden.

In this paper, we attempt to remedy the above shortcomings by proposing an implementation of a single-hidden-layer neural network over an eXtremely Large (XL) Multiple Input Multiple Output (MIMO) communication system, leveraging rich scattering effects and tunable combining with nonlinear components. Our methodology is structured around the Extreme Learning Machine (ELM) framework which admits random parameters and contains a limited number of trainable weights that can be optimized in closed form [8]. In our XL-MIMO-ELM implementation, the random coefficients arise from channel fading and provide diversity for feature extraction, while the analog combining weights play the role of trainable weights optimized to provide accurate estimations. Nonlinear components are introduced in the XL Rx side ensuring that our ELM approach exhibits universal approximation capabilities, while the closed-form solution allows for fast training and inference within reasonable channel coherence time durations.

## II. ELM PRELIMINARIES

Consider a data set  $\mathcal{D} \triangleq \{(\mathbf{x}^{(i)}, t^{(i)})\}_{i=1}^D$  of  $D$  observation vectors  $\mathbf{x}^{(i)} \triangleq [x_1^{(i)}, \dots, x_d^{(i)}]^\top \in \mathbb{R}^{d \times 1}$ , paired with their corresponding target values  $t^{(i)} \in \mathbb{R}$ . Let an ELM with  $K$  hidden nodes be defined via its trainable weight  $\mathbf{w} \triangleq [w_1, \dots, w_K]^\top \in \mathbb{R}^{K \times 1}$  in the output layer and random hidden layer coefficients  $\mathbf{A} \triangleq [\mathbf{a}_1, \dots, \mathbf{a}_K]^\top \in \mathbb{R}^{K \times d}$  with  $\mathbf{a}_k \in \mathbb{R}^{d \times 1}$  and  $\mathbf{b} \triangleq [b_1, \dots, b_K]^\top \in \mathbb{R}^{K \times 1}$ , as well as an activation function  $g(\cdot)$ . The ELM paradigm approximates the mapping  $\mathbf{x}^{(i)} \rightarrow t^{(i)}$  as follows:

$$\hat{t}^{(i)} \triangleq \sum_{k=1}^K w_k g(\mathbf{a}_k^\top \mathbf{x}^{(i)} + b_k) = \mathbf{w}^\top g(\bar{\mathbf{A}} \bar{\mathbf{x}}^{(i)}), \quad (1)$$

so that  $\hat{t}^{(i)}$  is the ELM’s estimate of  $t^{(i)}$  given  $\mathbf{x}^{(i)}$  as input. For notational consistency with following sections, the random coefficients have been merged as  $\bar{\mathbf{A}} \triangleq [\mathbf{A}, \mathbf{b}] \in \mathbb{R}^{K \times (d+1)}$  in (1), while  $\bar{\mathbf{x}}^{(i)}$  is appended with 1 as  $\bar{\mathbf{x}}^{(i)} \triangleq [x_1^{(i)}, \dots, x_d^{(i)}, 1]^\top \in \mathbb{R}^{(d+1) \times 1}$ . Let  $\mathbf{G} \in \mathbb{R}^{D \times K}$  denote

This work has been supported by the SNS JU project 6G-DISAC under the EU’s Horizon Europe research and innovation program under Grant Agreement No 101139130.

the output of the hidden layer for all data set points as  $\mathbf{G} \triangleq [g(\mathbf{A}\mathbf{x}^{(1)} + \mathbf{b}), \dots, g(\mathbf{A}\mathbf{x}^{(D)} + \mathbf{b})]^\top$ , and similarly, let  $\mathbf{t} \triangleq [t^{(1)}, \dots, t^{(D)}]^\top \in \mathbb{R}^{D \times 1}$ . Training an ELM involves finding the optimal weight vector  $\mathbf{w}^*$  that results in the minimum prediction error over  $\mathcal{D}$ , i.e.:

$$\mathbf{w}^* \triangleq \underset{\mathbf{w}}{\operatorname{argmin}} \|\mathbf{G}\mathbf{w} - \mathbf{t}\|. \quad (2)$$

Following [8, Eq. (13) and Thm. 5.1], the Least Squares (LS) solution of the latter linear system is given as follows:

$$\mathbf{w}^* = \mathbf{G}^\dagger \mathbf{t}, \quad (3)$$

where  $\mathbf{G}^\dagger$  is the Moore-Penrose generalized inverse of  $\mathbf{G}$ .

**Remark 1.** The LS solution of (3) results to  $\mathbf{w}^*$  having the smallest norm among all possible LS solutions of (2).

**Remark 2.** The time complexity for obtaining the solution of (3) is  $O(DK^2) + O(KD) = \Theta(DK^2)$ . The dominant term results from the Singular Value Decomposition (SVD) process in obtaining  $\mathbf{G}^\dagger$ , assuming  $D \geq K$ .

Compared to other ML models, ELMs have the advantage of containing few trainable weights (typically even  $K \leq D$ ) which can be obtained in closed form via (3) with small computational requirements. Besides, notwithstanding their random coefficients, an ELM with at most  $D$  trainable weights is a universal approximator [8], [9]. Precisely, [8, Thm's. 2.1 and 2.2] state that, for randomly chosen  $\mathbf{A}$  and  $\mathbf{b}$ ,  $\|\mathbf{G}\mathbf{w}^* - \mathbf{t}\| < \epsilon$  with probability one for arbitrarily small  $\epsilon > 0$ . The conditions for the universal approximation properties, which will be revisited later in this paper, are listed as follows:

**Condition 1.**  $\mathbf{A}$  and  $\mathbf{b}$  are independent and identically distributed (i.i.d.) samples of any continuous probability distribution with infinite support over  $\mathbb{R}^{K \times d}$  and  $\mathbb{R}^{K \times 1}$ , respectively.

**Condition 2.**  $g(\cdot)$  is an infinitely differentiable nonlinear function. Further conditions on the activation functions are imposed by [9], stating  $g(x)$  to be bounded and the limit as  $x \rightarrow \infty$  or  $x \rightarrow -\infty$  to exist.

### III. XL MIMO SYSTEMS AS ELMs

#### A. MIMO Channel Model

Let us consider an XL MIMO system with  $N_t$  Tx antenna elements and  $N_r$  Rx metamaterial-based antennas [10]. Let  $\mathbf{s} \triangleq [s_1, \dots, s_{N_t}]^\top \in \mathbb{C}^{N_t \times 1}$  be the transmitted signal and  $\tilde{\mathbf{n}} \sim \mathcal{CN}(\mathbf{0}, \sigma^2 \mathbf{I}) \in \mathbb{C}^{N_r \times 1}$  be the Additive White Gaussian Noise (AWGN) vector. We consider Ricean fading, according to which the channel matrix  $\mathbf{H} \in \mathbb{C}^{N_r \times N_t}$  is defined as:

$$\mathbf{H} \triangleq \sqrt{\frac{\kappa}{1+\kappa}} \sqrt{P_L} \mathbf{H}_{\text{LoS}} + \sqrt{\frac{1}{1+\kappa}} \sqrt{P_L} \mathbf{H}_{\text{NLoS}}, \quad (4)$$

where  $\kappa$  is the Ricean factor,  $P_L$  is the pathloss,  $\mathbf{H}_{\text{LoS}}$  is the Line-of-Sight (LoS) component, and  $\mathbf{H}_{\text{NLoS}}$  is the Non-Line-of-Sight (NLoS) component. The former matrix is defined as  $\mathbf{H}_{\text{LoS}} \triangleq \mathbf{a}_r(\theta_r) \mathbf{a}_t^H(\theta_t)$ , where  $\mathbf{a}_t(\theta_t) \in \mathbb{C}^{N_t \times 1}$  and  $\mathbf{a}_r(\theta_r) \in \mathbb{C}^{N_r \times 1}$  are respectively the Tx and Rx steering vectors, which, for Uniform Linear Arrays (ULAs), are expressed as:

$$\mathbf{a}_t(\theta_t) \triangleq \frac{1}{\sqrt{N_t}} [1, e^{j2\pi \frac{d_a}{\lambda} \sin(\theta_t)}, \dots, e^{j2\pi (N_t-1) \frac{d_a}{\lambda} \sin(\theta_t)}]^\top, \quad (5)$$

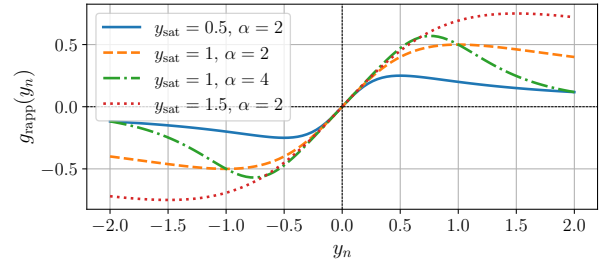


Fig. 1: Soft thresholding response via Rapp's model [11] used as the activation function for our XL-MIMO-ELM implemented directly with RF circuitry.

$$\mathbf{a}_r(\theta_r) \triangleq \frac{1}{\sqrt{N_r}} [1, e^{j2\pi \frac{d_a}{\lambda} \sin(\theta_r)}, \dots, e^{j2\pi (N_r-1) \frac{d_a}{\lambda} \sin(\theta_r)}]^\top, \quad (6)$$

where  $\theta_t$  and  $\theta_r$  are the angles of departure and arrival, respectively,  $d_a$  is the spacing between antennas, and  $\lambda$  is the signal wavelength. We make the typical assumption that the entries of  $\mathbf{H}_{\text{NLoS}}$  are sampled from  $\mathcal{CN}(0, 1/\sqrt{N_r N_t})$ . The baseband representation of the received signal  $\mathbf{y} \triangleq [y_1, \dots, y_{N_r}]^\top \in \mathbb{C}^{N_r \times 1}$  at the Rx metasurface-based antennas is expressed as:

$$\mathbf{y} \triangleq \mathbf{H}\mathbf{s} + \tilde{\mathbf{n}}. \quad (7)$$

#### B. Analog Combining with Nonlinear Soft Thresholding

The Rx structure is instrumental in our vision for XL MIMO systems realizing OTA ELM. In this section, we discuss the nonlinear operation that needs to take place before analog combining, leaving its detailed implementation for the journal version of this work. At the Rx, assume that each  $y_n$  from (7) is independently passed through a basic nonlinear component implementing soft thresholding. For example, using Rapp's model [11], its transfer function can be expressed as follows:

$$g_{\text{rapp}}(y_n) \triangleq y_n (1 + (y_n/y_{\text{sat}})^\alpha)^{-1}, \quad (8)$$

where  $y_{\text{sat}}$  is a saturation signal threshold, while  $\alpha$  controls the effect of the nonlinearity. Note that this model can capture the transfer function properties of various circuits, such as low-noise, variable-gain, or automatic gain control amplifiers. The exact details of such Radio Frequency (RF) components are left purposely unspecified, as designing components that best addresses the needs of XL-MIMO-ELMs opens a new direction of research. An illustration of different instances of  $g_{\text{rapp}}(y_n)$  for various values of  $y_{\text{sat}}$  and  $\alpha$  is given in Fig. 1. In the sequel, we choose  $|y_{\text{sat}}| = 1.5$  and  $\alpha = 2$  to obtain an activation function in  $[-1, 1]$  that mimics the shape of the sigmoid function  $1/(1 + \exp(-x))$ , and is thus convenient for binary classification problems, as considered in this paper.

The output of  $g_{\text{rapp}}(y_n)$  is then multiplied by a complex weight  $q_n$  capable of joint phase-amplitude control. We assume that both latter operations are realized by each meta-material element at the Rx [12]. Then, all weighted received signals are guided to the analog combiner to obtain the output of the XL MIMO system, using  $\mathbf{q} \triangleq [q_1, \dots, q_{N_r}]^\top$ , as:

$$z \triangleq \sum_{n=1}^{N_r} q_n g_{\text{rapp}}(y_n) = \mathbf{q}^\top g_{\text{rapp}}(\mathbf{y}). \quad (9)$$

Finally,  $z$  is downconverted and passed through a single Analog-to-Digital Converter (ADC), which significantly reduces the Rx hardware complexity. For classification settings where  $z \in \{0, 1, \dots, n_{\text{class}} - 1\}$ , an ADC with  $n_{\text{class}}$  quantization levels can be used to obtain the final class index.

### C. Proposed XL-MIMO-ELMs

Having described the computation framework of ELMs, a conventional XL-MIMO channel model, and the proposed nonlinear analog combining procedure, we are in position to describe how such a system can be used to perform training and OTA inference. Let us consider again the  $i$ -th observation vector of  $\mathcal{D}$ , once appended with 1 as its final element, i.e.,  $\bar{\mathbf{x}}^{(i)}$ . Without performing any encoding operations at the Tx, each element of  $\bar{\mathbf{x}}^{(i)}$  is transmitted by a corresponding Tx antenna, i.e.,  $\mathbf{s}^{(i)} \equiv \bar{\mathbf{x}}^{(i)}$ , signifying that  $d+1$  Tx antennas are required. It is noted that, since the data set and the corresponding ELM operations were defined for real-valued numbers to be more aligned with the majority of the benchmark data sets as well as the existing ELM theory, we only consider the real parts of the signals and channels in our investigations. More elaborate modulation and transmission schemes will be theoretically analyzed in the journal version of this paper.

We now focus on the high Signal-to-Noise Ratio (SNR) regime, where the AWGN term of (7) can be ignored. The following numerical evaluation provides empirical demonstration of the SNR effects on the devised approach. Combining (7) and (9), the output of the system is expressed as follows:

$$z^{(i)} = \mathbf{q}^\top g_{\text{rapp}}(\Re\{\mathbf{H}\}\bar{\mathbf{x}}^{(i)}). \quad (10)$$

Juxtaposing (10) with (1), it becomes evident that the proposed XL MIMO system performs computations equivalent to those of an ELM, where the size of its hidden layer corresponds to the number  $N_r$  of Rx antennas, and the trainable weights are implemented via the combiner vector. In particular, the random realizations of  $\mathbf{H}$  act as the randomized linear hidden-layer coefficients  $\bar{\mathbf{A}}$  of the ELM, so that the operation  $\mathbf{a}_k^\top \mathbf{x}^{(i)} + b_k$  takes place OTA by the wireless medium. As previously stated,  $g_{\text{rapp}}(\cdot)$  plays the role of the nonlinear activation function  $g(\cdot)$ . Crucially, the analog combining weights  $\mathbf{q}$  are the only trainable components of the system, akin to the weights of the output ELM layer  $\mathbf{w}$ . In that respect,  $z^{(t)} \equiv \hat{t}^{(i)}$  constitutes the estimation of the  $t^{(i)}$  by the XL-MIMO-ELM. The optimal combiner  $\mathbf{q}^*$  with respect to  $\mathcal{D}$  can be therefore obtained via the LS solution of (3), upon constructing the hidden output matrix  $\mathbf{G}$  for the whole data set, for fixed  $\mathbf{H}$ . Proceeding, the theoretical approximation guarantees of the proposed XL-MIMO-ELM implementation require investigation, for the particular selection of activation function and channel model. To this end, we provide the following theoretical result.

**Proposition 1.** *Consider the ELM expressed via (10), with  $\Re\{\mathbf{H}\}$  following Ricean fading and the Rapp activation function of (8) with  $\alpha \in \mathbb{N}_+ \setminus \{1\}$ . Then, given any arbitrarily small value  $\epsilon > 0$ , there exists  $N_r \leq D$  such that, for  $D$*

*arbitrary distinct samples  $\{(\mathbf{x}^{(i)}, t^{(i)})\}_{i=1}^D$ , there exists  $\mathbf{q}^*$  so that  $\|\mathbf{G}\mathbf{q}^* - \mathbf{t}\| < \epsilon$  with probability one.*

*Proof.* The proof follows the direct application of [8, Thm 2.2] and the activation function requirements of [9], upon ensuring that Conds. 1 and 2 are satisfied. The Ricean distribution of (4) on  $\mathbf{H}$  is continuous ensuring that  $\Re\{\mathbf{H}\}$  can be sampled in any interval in  $\mathbb{R}^{N_r \times N_t}$  with nonzero probability, which fulfills Cond. 1. Additionally, the Rapp activation function of (8) is nonlinear and infinitely differentiable with respect to  $y_n$ , as long as  $\alpha \in \mathbb{N}^+$ . Furthermore,  $\lim_{y_n \rightarrow \infty} g_{\text{rapp}}(y_n) = 0$  for  $\alpha > 1$ , due to the dominance of the denominator. Regarding boundedness for  $y_n \in (0, +\infty)$ ,  $dg_{\text{rapp}}/dy_n = y_{\text{sat}}^\alpha (y_{\text{sat}}^\alpha + (1-\alpha)y_n^\alpha) / (y_{\text{sat}}^\alpha + y_n^\alpha)^2 = 0$  provides a unique solution at  $y_n^* = y_{\text{sat}}(\alpha-1)^{-1/\alpha}$ . Moreover,  $g_{\text{rapp}}(y_n^*) = \frac{y_{\text{sat}}}{\alpha}(\alpha-1)^{1-\frac{1}{\alpha}}$  is a finite maximum value. Following the same arguments for  $y_n \in (-\infty, 0)$  and by noting that  $g_{\text{rapp}}(0) = 0$ ,  $g_{\text{rapp}}(\cdot)$  is bounded everywhere. As a result, Cond. 2 holds for the Rapp activation function, which completes the proof.  $\square$

## IV. DISCUSSION AND FUTURE WORK

In the proposed XL-MIMO-ELM framework, no computation takes place at the Tx, since all operations happen either OTA or via the nonlinear analog combining at the XL Rx, which simplifies its requirements for edge inference tasks. Remark 1 implies that the optimization procedure automatically minimizes the power consumption at the Rx, since the norm of the combiner (trainable weight) corresponds to the reception power. Extensions of this work will focus on devising advanced transmission schemes exploiting frequency and temporal degrees of freedom, or adopting illumination strategies similar to [2] for parallelizing the transmission of the input elements without digital Tx-side processing, thus, reducing the required numbers (i.e.,  $d+1$ ) of Tx antennas.

While the Ricean fading model satisfies Cond. 1, the proof of [8, Thm. 2.2] relies in constructing high-rank instances of  $\mathbf{G}$  that result in highly expressive random bases. In LoS-dominant scenarios with large  $\kappa$  values, the channel may not exhibit high enough diversity to ensure favorable matrices. As a result, higher  $N_r$  values might be required to obtain linearly independent random coefficients that contain sufficient representation power. As a result, the proposed scheme is expected to be more effective in rich scattering environments. The following numerical evaluation investigates the performance of XL-MIMO-ELM under increasing LoS conditions.

An implication of the presented methodology is that the  $\mathbf{H}$  matrix remains constant both during training as well as during inference, where the system is used to make estimations on new data points. While the optimization process is fast enough to be completed within reasonably long channel coherent blocks, ensuring constant channel at every time instance inference is difficult in standard wireless communication environments. In this perspective, the proposed framework is better equipped for inference on fast streams of data, where the target values of a portion of the data set are unknown. Such scenarios

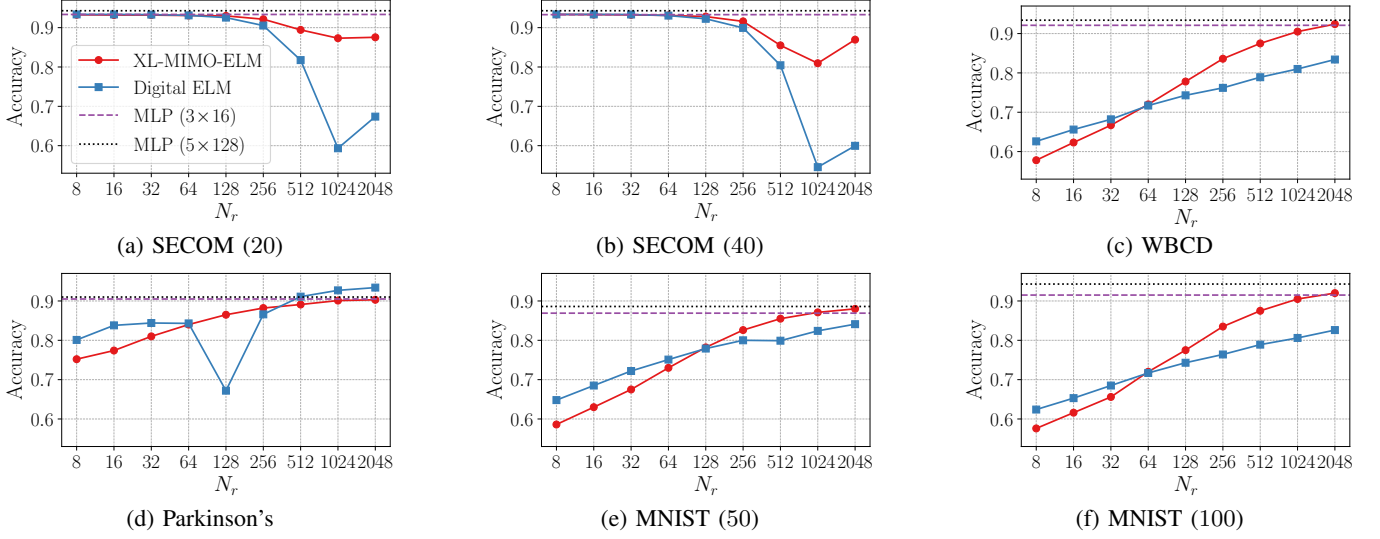


Fig. 2: Comparative performance of the proposed XL-MIMO-ELM with benchmarks across different datasets for increasing number of Rx antennas  $N_r$  (implying the number of units in the hidden layer).

can be frequently found in industrial applications and sensor networks [13], where real-time decision making is paramount.

As an alternative direction, the implementation of an XL-MIMO-ELM system may be based on a purposely manufactured and controlled environment that ensures rich, yet static, fading, instead of utilizing conventional environments met in wireless communications. This idea paves the way for wave-domain computing as a candidate physical implementation of ML models. In fact, by exploiting diffractive metamaterial technology, such as Stacked Intelligent Metasurfaces (SIMs) [14] that have been shown capable of performing a variety of computational operations [1], [5], the nonlinear activation and analog combining operations at the Rx could be implemented directly OTA, providing exciting future continuations of this work. Such approaches may also enable cascades of multi-layered ELMs [15], [16] for wave-domain deep learning. Finally, as a side contribution of this work, the introduced theoretical guarantees provide insights on the approximation capabilities and performance of deep learning approaches over the channel, such as [5], [6], where random channel matrices are treated as hidden neural network units.

## V. NUMERICAL EVALUATION

We conduct a numerical evaluation of the proposed XL-MIMO-ELM with simulated channels on common numerical binary classification data sets of small-to-medium size, so that training can be reasonably be assumed to take place within the channel coherence time. Specifically, *i*) the Parkinson's data set [17], composed of a range of biomedical voice of potential patients with Parkinson's disease and comprising 191 instances with 22 features; *ii*) the Wisconsin Breast Cancer Diagnostic (WBCD) data set [18], comprising 569 instances of 30 features from images of a fine needle aspirate of a breast mass; *iii*) two variations of the SECOM data set, which contains 591 features of potentially noisy signals from semiconductor manufacturing process sensors for 1567 instances

to be classified according to pass/fail yields for in-house line testing: SECOM (20) and SECOM (40) including only 20 and 40 randomly selected features, respectively; and *iv*) two cases of MNIST classification [19] of  $6 \times 10^4$  handwritten digit images, where 50 and 100 pixels (features) have been randomly sampled as features and the problem was converted as binary classification by predicting whether each image contains an even or odd digit. An 80 : 20 training-test split was applied, and all features have been independently standardized to zero mean and unit variance. The considered benchmarks include: *i*) a conventional ELM algorithm (referred to as "Digital ELM") using sigmoid activation and uniformly random hidden layer coefficients  $\mathbf{A}$ ,  $\mathbf{b}$  in  $[0,1]$ ; *ii*) a Multi-Layer Perceptron (MLP) of 3 layers of 32 neurons; as well as *iii*) a larger MLP with 5 layers of 128 neurons. Notice that the two MLPs have approximately  $2.8 \times 10^3$  to  $5.3 \times 10^3$  and  $6.9 \times 10^4$  to  $7.9 \times 10^4$  trainable parameters, respectively, depending on the data set, while the considered ELMs have only up to 2048.

The mean test set classification accuracy over 200 random seeds for the considered methods for all data sets is given in Fig. 2 over increasing numbers  $N_r$  of Rx antennas (i.e., ELM trainable parameters). As expected from the theoretical analysis, as the number of hidden neurons increases, both ELMs achieve results comparable to the MLPs, which have orders of magnitude more parameters. Across all data sets, the performance of XL-MIMO-ELM is at the same level, or better, than the digital ELM variation with the same number of parameters, since the latter sparsely exhibits unstable performance at certain  $N_r$  values. We attribute this behavior to the larger variance of the uniform coefficients compared to Ricean fading. Proceeding, we conduct further investigations on the effect of wireless parameters on the ELM for three of the data sets and two  $N_r$  values. First, we sample i.i.d. AWGN instances for every computation of (7), i.e., both during the construction of  $\mathbf{G}$  and during inference on unseen



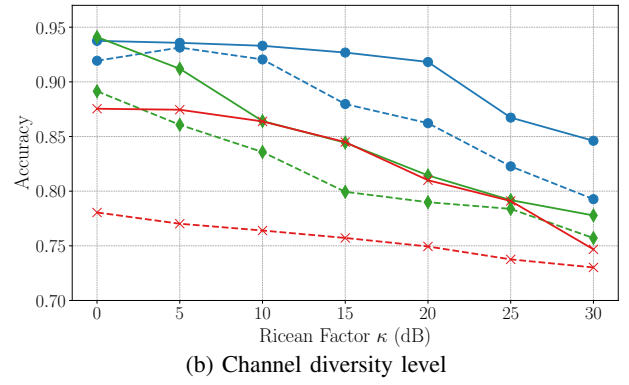
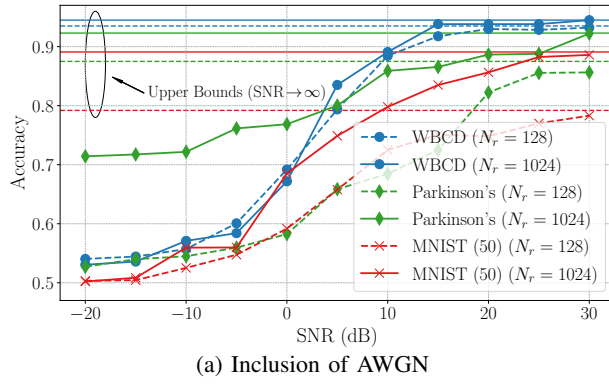


Fig. 3: Performance of various XL-MIMO-ELM settings on different data sets versus numbers  $N_r$  of Rx antennas.

data, with  $\sigma^2$  values so that the receive SNR results in pre-defined levels; the receive-SNR is measured by the total channel gain as  $\gamma \triangleq \bar{P} \|\mathbf{H}\|_F^2 / (N_t \sigma^2)$ , where  $\bar{P} \triangleq \mathbb{E}[\|\bar{\mathbf{x}}\|^2]$  is the mean transmission power. Figure 3a shows the effect of the SNR level on the classification accuracy. It can be seen that as this level increases, the performance of the proposed approach under all system parameters (data set and  $N_r$ ) approaches the performances of its idealized case counterpart (Fig. 2), demonstrating the validity of the high-SNR analysis conducted. Finally, Fig. 3b examines the effects of multipath on XL-MIMO-ELM for the same cases as in Fig. 3a. As discussed, rich scattering conditions provide more favorable distributions with enough diversity for accurate classification, while results degrade as the dominance of the LoS component increases. Larger antenna numbers seem to provide a level of tolerance to high Ricean  $\kappa$ -factor conditions, however, the performance loss is still noticeable.

## VI. CONCLUSION

This paper presented the implementation of the ELM algorithm for OTA training and inference, leveraging the similarities between wireless propagation characteristics and Rx analog combining operations within the ELM framework. An analog activation function modeling soft thresholding was proposed, and the conducted theoretical analysis confirmed the implementation to preserve the universal approximation capabilities of the original ELM framework. The impact of system characteristics was discussed, and potential exciting future research directions were highlighted. The findings were further validated through numerical evaluation, which demonstrated that the proposed XL-MIMO-ELM achieves performance on par with the original ELM algorithm and benchmarks containing larger numbers of parameters.

## REFERENCES

- [1] Z. R. Omam *et al.*, “Holographic metasurfaces enabling wave computing for 6G: Status overview, challenges, and future research trends,” *arXiv preprint arXiv:2501.05173*, 2025.
- [2] X. Lin *et al.*, “All-optical machine learning using diffractive deep neural networks,” *Science*, vol. 361, no. 6406, pp. 1004–1008, 2018.
- [3] A. Momeni and R. Fleury, “Electromagnetic wave-based extreme deep learning with nonlinear time-floquet entanglement,” *Nature Commun.*, vol. 13, no. 1, p. 2651, May 2022.
- [4] P. Di Lorenzo *et al.*, “Goal-oriented communications for the IoT: System design and adaptive resource optimization,” *IEEE Internet Things Mag.*, vol. 6, no. 4, pp. 26–32, 2023.
- [5] K. Stylianopoulos *et al.*, “Over-the-air edge inference via metasurfaces-integrated artificial neural networks,” *arXiv preprint arXiv:2504.00233*, 2025.
- [6] H. Ye *et al.*, “Deep over-the-air computation,” in *Proc. IEEE Int. Conf. Commun.*, virtual, 2020.
- [7] G. Huang *et al.*, “Stacked intelligent metasurfaces for task-oriented semantic communications,” *arXiv preprint arXiv:2407.15053*, 2024.
- [8] G.-B. Huang *et al.*, “Extreme learning machine: Theory and applications,” *Neurocomput.*, vol. 70, no. 1, pp. 489–501, Dec. 2006.
- [9] G.-B. Huang and H. Babri, “Upper bounds on the number of hidden neurons in feedforward networks with arbitrary bounded nonlinear activation functions,” *IEEE Trans. Neural Netw.*, vol. 9, 1998.
- [10] N. Shlezinger *et al.*, “Dynamic metasurface antennas for 6G extreme massive mimo communications,” *IEEE Wireless Commun.*, vol. 28, no. 2, pp. 106–113, 2021.
- [11] C. Rapp, “Effects of HPA-nonlinearity on a 4-DPSK/OFDM-signal for a digital sound broadcasting signal,” in *ESA Special Publications Series*, B. Kaldeich, Ed., vol. 332, 1991, pp. 179–184.
- [12] P. Gavrilidis *et al.*, “Active reconfigurable intelligent surfaces: Circuit modeling and reflection amplification optimization,” *arXiv preprint arXiv:2503.24093*, 2025.
- [13] M. McCann and A. Johnston, “SECOM: Data from a semi-conductor manufacturing process,” UC Irvine Machine Learning Repository, 2008, doi: 10.24432/C54305.
- [14] J. An *et al.*, “Stacked intelligent metasurfaces for efficient holographic MIMO communications in 6G,” *IEEE J. Sel. Areas Commun.*, vol. 41, no. 8, pp. 2380–2396, 2023.
- [15] S. Ding *et al.*, “Deep extreme learning machine and its application in EEG classification,” *Math. Problems Eng.: Extreme Learning Machine on High Dimensional and Large Data Appl.*, 2015.
- [16] G. Altan and Y. Kutlu, “Superiorities of deep extreme learning machines against convolutional neural networks,” *Natural Eng. Sci.*, vol. 3, pp. 103–109, 2018.
- [17] M. A. Little *et al.*, “Suitability of dysphonia measurements for telemonitoring of Parkinson’s disease,” *IEEE Trans. Biomed. Eng.*, vol. 56, no. 4, pp. 1015–1022, 2009.
- [18] W. Wolberg *et al.*, “Diagnostic Wisconsin breast cancer database,” UC Irvine Machine Learning Repository, 2008, doi: 10.24432/C5DW2B.
- [19] L. Deng, “The MNIST database of handwritten digit images for machine learning research,” *IEEE Signal Process. Mag.*, vol. 29, no. 6, pp. 141–142, 2012.